Towards a Unified Approach for Continuously-Variable Impedance Control of Powered Prosthetic Legs over Walking Speeds and Inclines

Albert J. Lee, Curt A. Laubscher, T. Kevin Best and Robert D. Gregg

***Abstract*— Research in powered prosthesis control has explored the use of impedance-based control algorithms due to their biomimetic capabilities and intuitive structure. Modern impedance controllers feature parameters that smoothly vary over gait phase and task according to a data-driven model. However, these recent efforts only use continuous impedance control during stance and instead utilize discrete transition logic to switch to kinematic control during swing, necessitating two separate models for the different parts of the stride. In contrast, this paper presents a controller that uses smooth impedance parameter trajectories throughout the gait, unifying the stance and swing periods under a single, continuous model. Furthermore, this paper proposes a basis model to represent inter-task relationships in the impedance parameters—a strategy that has previously been shown to improve model accuracy over classic linear interpolation methods. In the proposed controller, a weighted sum of Fourier series is used to model the impedance parameters of each joint as continuous functions of gait cycle progression and task. Fourier series coefficients are determined via convex optimization such that the controller best reproduces the joint torques and kinematics in a reference able-bodied dataset. Experiments with a powered knee-ankle prosthesis show that this simpler, unified model produces competitive results when compared to a more complex hybrid impedance-kinematic model over varying walking speeds and inclines.**

I. INTRODUCTION

Many daily activities, such as incline walking and stair ascent, require positive power input from the knee and ankle at various points in the gait cycle [1], [2]. As such, transfemoral amputees with passive prostheses experience disadvantages and often suffer from issues like increased energy consumption and irregular walking behaviors [3], [4]. Powered prostheses could avoid these problems by injecting energy at appropriate points in the gait.

The usage of active devices begs the question of how to properly control them. Some efforts have focused on phase-based kinematic control, where the knee and ankle are controlled to follow position trajectories that mimic able-bodied motion [5]–[7]. While these controllers are capable of generating appropriate kinematic trends and use a single controller over the entire stride [5], they fail to reproduce able-bodied kinetics. This limitation has resulted in recent efforts focusing on impedance control methods due to their ability to mimic able-bodied angles and torques, generate compliant interaction between the prosthesis and the ground, and accurately model joint behavior [8]–[11]. Impedance control calculates joint torque $\hat{\tau}$ by the expression

$$\hat{\tau} = K(\theta_{\text{eq}} - \theta) - B\dot{\theta}, \tag{1}$$

where K, θ_{eq}, and B are stiffness, equilibrium angle, and damping terms, respectively, and θ and $\dot{\theta}$ represent the joint position and velocity. A common implementation of impedance control uses a finite state machine, where the stride is discretized into several states. Each state has its own set of tuned impedance parameters [12]–[14]. However, this approach results in a large number of adjustable values (i.e., impedance parameters for each activity, transition criteria between states within the stride, etc.), meaning that tuning the controller is prohibitively time-intensive.

To address this limitation, several researchers have modeled the impedance parameters as continuous functions of gait phase. In these controllers, impedance control is often limited to the stance period, while swing is dictated by a position controller. One example [15] used a model that defines stiffness and damping as hand-tuned linear functions that do not change with task. Developments on this idea began using able-bodied data to identify polynomial functions for the stiffness and damping parameters [16], [17]. These works still chose to use a piecewise-constant function for θ_{eq}, and while [17] captures parameter changes due to incline, it does not address changes due to walking speed. Recently, [18] introduced a continuous impedance model of stiffness, damping, and equilibrium angle as continuous functions of phase during the stance period of walking. This model generated impedance parameter trajectories for a range of inclines and speeds and displayed state-of-the-art levels of biomimicry across these tasks. This control architecture was then extended to stair ascent and descent over various step heights [19].

However, by using a hybrid combination of impedance control during stance and position control during swing, the control architecture in [18], [19] still requires discrete transitions and multiple models to describe the gait. We hypothesize that this approach is more complex than necessary, and that the full stride can instead be described by a single model. Furthermore, [18] uses linear interpolation to determine impedance parameters for tasks that are not in the training set, even though previous results have shown improvement in cross-task modeling when using continuous task functions rather than linear interpolation [6].

In an effort to address these limitations, the proposed controller—hereafter referred to as the Full Stride Impedance Controller (FSIC)—uses a single continuous model for the entire walking stride. The controller computes output torques

This work was supported by the National Institute of Child Health & Human Development of the NIH under Award Number R01HD094772.

All authors are with the Department of Robotics, University of Michigan, Ann Arbor, MI 48109. Contact: {albjlee, claub, tkbest, rdgregg}@umich.edu

using the impedance model described in (1), with the parameters K, B, and θ_{eq} being chosen such that the controller produces biomimetic torques during stance, then angle-tracking torques during swing. Additionally, the FSIC repurposes the basis structure described in [6] to model impedance parameter behavior across tasks. In doing so, we explore the potential for improved cross-task modelling of impedance parameters over classic linear interpolation techniques. After a series of bypass experiments comparing the FSIC with a benchmark hybrid impedance-kinematic controller, we conclude that the proposed control method achieves near-cutting-edge performance with a unified control scheme that operates continuously over the entire gait without the need for discrete transitions or multiple models.

II. Methodology

A. Modeling Framework

The model described in [6] has a mathematical structure that is well-suited for full-stride models and is continuous in each of the task dimensions. We apply this model to the impedance control strategy detailed in [18] with the aims of (a) expanding the control method to the entire gait cycle and (b) better representing cross-task trends.

Stiffness $K(\phi, \chi)$, damping $B(\phi, \chi)$, and equilibrium angle $\theta_{\text{eq}}(\phi, \chi)$ are modeled as continuous, smooth functions of gait phase ϕ and task χ. Gait phase ϕ is a periodic scalar value that monotonically increases from 0 to 1 throughout each stride. It can be estimated in real-time via a phase variable. The task vector χ contains the user's current walking speed ν and incline ϵ, each linearly mapped from physical units (i.e., [0.8 m/s, 1.2 m/s] and [-10°, 10°]) to the range [0, 1]. The expressions for each parameter are given as

$$\begin{gathered} K = \sum_{l=1}^{N} C_l(\chi) k_l(\phi), \quad B = \sum_{l=1}^{N} C_l(\chi) b_l(\phi), \\ \theta_{\text{eq}} = \sum_{l=1}^{N} C_l(\chi) e_l(\phi) \end{gathered} \tag{2}$$

where $N = 7$ denotes the number of task functions C_l.

The task functions C_l are Bernstein polynomials that apply weights to the parameter-specific functions $k_l(\phi)$, $b_l(\phi)$, and $e_l(\phi)$. Bernstein polynomials have been shown to better represent cross-task kinematic trends compared to linear interpolation [6]. We hypothesize that this property will also apply to impedance parameter modeling. Each task function $C_l(\chi)$ is defined as

$$C_l(\chi) = \binom{d}{q} f(\chi)^q (1 - f(\chi))^{d-q},$$

where the index l specifies which of three subgroups a given task function belongs to. Each subgroup dictates the values of d, q, and $f(\chi)$ as

$$\begin{aligned} l &= 1 && \Rightarrow d = 0, q = 0, f = 0 \\ l &= 2, 3, 4 && \Rightarrow d = 2, q = l - 2, f = \nu \\ l &= 5, 6, 7 && \Rightarrow d = 2, q = l - 5, f = \epsilon \end{aligned} \tag{3}$$

The first subgroup provides a constant function, the second establishes functions that capture changes in the parameters due to walking speed, and the third does the same for changes in incline. The exact values of each parameter were chosen empirically. Note that in this context, we define $0^0 = 1$.

The basis functions $k_l(\phi), b_l(\phi)$, and $e_l(\phi)$ are defined as Fourier series, which were chosen for their periodic nature and the periodicity of gait. The functions k_l are defined as:

$$k_l(\phi) = \alpha_{00l} + \sum_{m=1}^{F} \alpha_{1ml} \cos(2\pi m \phi) + \alpha_{2ml} \sin(2\pi m \phi). \tag{4}$$

The functions for damping $b_l(\phi)$ and equilibrium angle $e_l(\phi)$ are defined similarly, each parameterized by coefficients β_{iml} and γ_{iml}, respectively. The series orders were heuristically selected to be $F = 4$ for the ankle and $F = 6$ for the knee.

B. Model Fitting Objectives and Constraints

The model parameters $(\alpha_{iml}, \beta_{iml}, \gamma_{iml})$ are determined via convex optimization, using an able-bodied dataset [2] as reference. The objectives of the optimization vary over the course of the stride, as will be described in sections II-B.2 and II-B.3. In an effort to frame this model as a convex quadratic program (QP), we first present a change-of-variables and model approximation.

1) Convex Approximation: Previous efforts to use convex optimization to solve for impedance parameter models have shown that the product $K\theta_{\text{eq}}$ leads to nonconvexities in torque error minimization problems, making them difficult to solve [18]–[20]. To avoid this, we introduce the change of variables $P = K\theta_{\text{eq}}$ as done in [18]:

$$\begin{aligned} P = K\theta_{\text{eq}} &= \left(\sum_{l=1}^{N} C_l(\chi) k_l(\phi) \right) \left(\sum_{l=1}^{N} C_l(\chi) e_l(\phi) \right), \\ &= \sum_{l=1}^{N} \sum_{r=1}^{N} C_l(\chi) C_r(\chi) k_l(\phi) e_r(\phi), \\ &= \sum_{l=1}^{N} \sum_{r=1}^{N} C_l(\chi) C_r(\chi) p_{l,r}(\phi), \text{where} \end{aligned} \tag{5}$$

$$p_{l,r} = \delta_{00lr} + \sum_{m=1}^{2F} \delta_{1mlr} \cos(2\pi m \phi) + \delta_{2mlr} \sin(2\pi m \phi). \tag{6}$$

During evaluation, we can recover the original model by approximating θ_{eq} as $\frac{P}{K}$.

We now collect the unknown model parameters for stiffness into a vector x_K as

$$x_K^l = \begin{bmatrix} \alpha_{00l} & \alpha_{11l} & \alpha_{21l} & \cdots & \alpha_{2Fl} \end{bmatrix}, \tag{7}$$

$$x_K = \begin{bmatrix} x_K^1 & x_K^2 & \cdots & x_K^N \end{bmatrix} \in \mathbb{R}^{1 \times N(2F+1)}. \tag{8}$$

Vectors x_B and x_P for the damping and product functions are defined similarly using their respective coefficients β_{iml} and δ_{imlr}. We can then write an argument vector $x \in \mathbb{R}^{2N(2F+1)+N^2(4F+1)}$ containing all of the unknown model parameters as $x = \begin{bmatrix} x_K & x_B & x_P \end{bmatrix}^\top$.

2) Stance Objective: The stance period's objective is to match the impedance model's output to able-bodied joint torques. This is achieved by minimizing $f_1(x)$:

$$f_1(x) = ||\lambda_1 \Lambda_{\text{st}}(\tau - \hat{\tau})||^2. \tag{9}$$

The term λ_1 is a diagonal weight matrix that determines the priority of this objective. We define λ_1 as a diagonal matrix rather than a scalar in order to permit varied weight definition within stance, which proved to be helpful for swing-stance transitions (described in section II-B.7). The constant Λ_{st} is a binary diagonal matrix that selects the rows of $\tau - \hat{\tau}$ that are associated with stance. This matrix is determined by using ground reaction force data. The vector τ is comprised of able-bodied torque data from full strides (each stride discretized into S phase timesteps) across all T tasks:

$$\tau = \begin{bmatrix}\tau_{\chi_1} & \tau_{\chi_2} & \cdots & \tau_{\chi_T}\end{bmatrix}^\top \in \mathbb{R}^{ST}, \text{where}$$
$$\tau_{\chi_j} = \begin{bmatrix}\tau_{1,j} & \tau_{2,j} & \cdots & \tau_{S,j}\end{bmatrix}^\top \in \mathbb{R}^{S}.$$

For clarity, we have defined $\tau_{i,j} = \tau_{\phi_i,\chi_j}$ and will use this notation for all other phase- and task-dependent parameters. Equivalently, $\hat{\tau}$ contains the impedance model's output for each of the strides across all the tasks:

$$\hat{\tau} = \begin{bmatrix}\hat{\tau}_{1,1} & \cdots & \hat{\tau}_{S,T}\end{bmatrix}^\top \in \mathbb{R}^{ST}, \text{where}$$
$$\hat{\tau}_{i,j} = P_{i,j} - K_{i,j}\theta_{i,j} - B_{i,j}\dot{\theta}_{i,j}.$$

P, K, and B are computed using (2) and (5). θ and $\dot{\theta}$ denote joint angles and velocities obtained from the dataset.

3) Swing Objectives: The swing period's objective is to generate biomimetic kinematic trajectories, rather than mimicking able-bodied torques (which, depending on the geometry and mass distribution of the prosthesis, may lead to aberrant behaviors). This is achieved by minimizing the difference between the equilibrium angle and joint kinematics. By driving θ_{eq} towards the desired trajectory of able-bodied kinematics (equivalently driving $K\theta - P$ to zero) and simultaneously releasing the torque-matching objective, we can encourage an impedance controller to behave similarly to a proportional-derivative position controller. This objective is addressed by minimizing $f_2(x)$:

$$f_2(x) = ||\lambda_2 \Lambda_{\text{sw}}(\overline{K\theta} - \overline{P})||^2.$$

As done in the stance objective, λ_2 is a diagonal matrix of phase-dependent weights and Λ_{sw} is a binary diagonal matrix that selects swing period data. $\overline{K\theta}$ and $\overline{P}$ are each vectors in $\mathbb{R}^{ST}$ populated with the relevant values for each parameter:

$$\overline{K\theta} = \begin{bmatrix}K_{1,1}\theta_{1,1} & K_{2,1}\theta_{2,1} & \cdots & K_{S,T}\theta_{S,T}\end{bmatrix}^\top,$$
$$\overline{P} = \begin{bmatrix}P_{1,1} & P_{2,1} & \cdots & P_{S,T}\end{bmatrix}^\top.$$

4) Rate-of-Change Objectives: In order to produce a comfortable walking stride, we made various assumptions about optimal behavior of the impedance parameters. Specifically, we believed that equilibrium angle should have low-frequency trajectories during stance, as previous hardware experiments showed us that high-frequency equilibrium angle trajectories resulted in user discomfort. This may be because the resulting output of the impedance model has a high-frequency feedforward component in the $K\theta_{\text{eq}}$ term, making any departure from the expected kinematics produce undesirable torques. We also assumed that stiffness and damping should have low frequencies during swing, since we sought to achieve kinematic tracking during that part of the stride. We believed that high-frequency stiffness and damping terms would result in a jittery, unstable torque output. While we did not devote major effort towards reaching a decisive conclusion about these assumptions (since answering these questions was not our ultimate goal), all three hypotheses were supported by hardware experiments.

We produce this period-specific behavior by punishing the derivatives of these parameters at appropriate gait phases. This cost component is defined as

$$f_3(x) = \lambda_3 \left\| \Lambda_{\text{st}} \overline{\frac{\partial P}{\partial \phi}} \right\|^2 + \lambda_4 \left\| \Lambda_{\text{sw}} \overline{\frac{\partial K}{\partial \phi}} \right\|^2 + \lambda_5 \left\| \Lambda_{\text{sw}} \overline{\frac{\partial B}{\partial \phi}} \right\|^2.$$

As in the previous objectives, $\overline{\frac{\partial P}{\partial \phi}}$, $\overline{\frac{\partial K}{\partial \phi}}$, and $\overline{\frac{\partial B}{\partial \phi}}$ are each $ST \times 1$ vectors populated by the derivatives evaluated at each timestep for each stride over all the tasks.

5) Regularization Objective: A regularization term was added to address overfitting, given by $f_4(x) = \lambda_6 ||x||^2$. The full objective function can now be expressed as the sum of each cost component $f_i(x)\ \forall i \in \{1, 2, 3, 4\}$.

6) Constraints: Phase-varying bounding constraints for K and B are introduced for each joint in order to ensure stable behavior. On top of this, to improve user confidence during the early phases of the stride (when the prosthesis rapidly takes on the user's weight), a weight-bearing stiffness constraint $K_{\text{min}}^{\text{WB}}$ is enforced immediately after the swing-stance transition region (described below in Section II-B.7). The values of each constraint are given in Table I. All stiffness constraints are given in Nm/rad/kg and all damping constraints are given in Nms/rad/kg.

7) Swing-Stance Transitions: To encourage a comfortable transition between the swing and stance periods (particularly in the knee), we heuristically chose appropriate values for the weighting matrices λ_1 and λ_2 used in objectives $f_1(x)$ and $f_2(x)$. Throughout swing, we penalize kinematic error with weight λ_2^{MS}, before modifying it at the final phase timestep to a heel strike value of $\lambda_2^{\text{HS}^-}$. Furthermore, the first 6.7% of stance phase has a torque objective weight λ_1^{ES}, while the remainder of stance has weight λ_1^{MS}. Stiffness is also unconstrained in this early stance region. These protocols result in more biomimetic, low-stiffness behaviors during late swing while still allowing for robust, high-stiffness performance during early stance.

C. Model Linearity and Objective Convexity

We now show that the impedance parameters and their partial derivatives can be expressed as linear functions of x. By doing so, we show that each element of the x-dependent vectors in the objectives—namely, $\hat{\tau}$, $\overline{K\theta}$, $\overline{P}$, $\overline{\frac{\partial P}{\partial \phi}}$, $\overline{\frac{\partial K}{\partial \phi}}$, and $\overline{\frac{\partial B}{\partial \phi}}$—are linear in x, and thus the objective functions $f_i(x)$ are quadratic in x. We show that the constraints are likewise

affine in x, and therefore the overall minimization problem can be solved as a standard quadratic program.

1) Model Linearity: Let a_ϕ contain the sinusoidal terms evaluated at ϕ, and A_ϕ be a block diagonal matrix:

$$a_\phi = \begin{bmatrix}1 & \cos(2\pi\phi) & \cdots & \sin(2\pi F\phi)\end{bmatrix} \in \mathbb{R}^{1\times 2F+1},$$
$$A_\phi = \text{blkdiag}(a_\phi) \in \mathbb{R}^{N\times N(2F+1)},$$

where the blkdiag() function denotes a block diagonal matrix with a_ϕ blocks along the diagonal and zeroes elsewhere. The $k_l(\phi)$ functions can now be written as a matrix product:

$$\begin{bmatrix}k_1(\phi) & k_2(\phi) & \cdots & k_N(\phi)\end{bmatrix}^\top = A_\phi^K x, \text{where}$$
$$A_\phi^K = \begin{bmatrix}A_\phi & \mathbf{0}_{N\times N(2F+1)} & \mathbf{0}_{N\times N^2(4F+1)}\end{bmatrix}.$$

The $b_l(\phi)$ functions can be computed similarly by left-multiplying x by $A_\phi^B = \begin{bmatrix}\mathbf{0} & A_\phi & \mathbf{0}\end{bmatrix}$. By defining a vector of task functions y_χ, the expressions for K and B in (2) can be written as matrix products that are linear in x:

$$y_\chi = \begin{bmatrix}C_1(\chi) & C_2(\chi) & \cdots & C_N(\chi)\end{bmatrix},$$
$$K = y_\chi A_\phi^K x \;\;;\;\; B = y_\chi A_\phi^B x. \tag{10}$$

Due to its framing as a product of the weighted sums of Fourier series, the expansion of P as a matrix product is different from the expressions for K and B. First, a vector a_ϕ^P and corresponding matrices $\bar{A}_\phi$ and A_ϕ^P are defined in order to accommodate the doubling in the Fourier series order:

$$a_\phi^P = \begin{bmatrix}1 & \cos(2\pi\phi) & \cdots & \sin(2\pi(2F)\phi)\end{bmatrix} \in \mathbb{R}^{1\times 4F+1},$$
$$\bar{A}_\phi = \text{blkdiag}(a_\phi^P) \in \mathbb{R}^{N^2\times N^2(4F+1)},$$
$$A_\phi^P = \begin{bmatrix}\mathbf{0}_{N^2\times N(2F+1)} & \mathbf{0}_{N^2\times N(2F+1)} & \bar{A}_\phi\end{bmatrix}.$$

After replacing the l, r subscripts in (6) with a single indexing variable l that ranges from 1 to N^2, we can express the p_l functions as follows:

$$\begin{bmatrix}p_1(\phi) & p_2(\phi) & \cdots & p_{N^2}(\phi)\end{bmatrix}^\top = A_\phi^P x.$$

We also generate a product of task matrices in order to fully express the double summation in (5):

$$P = y_\chi Y_\chi A_\phi^P x, \text{where}$$
$$Y_\chi = \text{blkdiag}(y_\chi) \in \mathbb{R}^{N\times N^2}. \tag{11}$$

Since all impedance parameters are linear in x, the impedance model output (which is linear in the parameters K, B and P) is also linear in x. The rate-of-change objectives (Section II-B.4) can be found by taking the elementwise partial derivatives of the A_ϕ matrices with respect to phase. The remainder of the derivations are analogous to those of the impedance parameters and have been omitted for brevity:

$$\frac{\partial K}{\partial \phi} = y_\chi \frac{\partial A_\phi^K}{\partial \phi} x \;\;,\;\; \frac{\partial B}{\partial \phi} = y_\chi \frac{\partial A_\phi^B}{\partial \phi} x \;\;,$$
$$\frac{\partial P}{\partial \phi} = y_\chi Y_\chi \frac{\partial A_\phi^P}{\partial \phi} x.$$

Note that $\frac{\partial}{\partial \phi}$ denotes elementwise differentiation.

To fully express this problem as a QP, the constraints must also be linear in x. We enforce the constraints by building a matrix D that, when multiplied by x, gives the stiffness and damping values over the full training space:

$$D = \begin{bmatrix}D_K^\top & D_B^\top\end{bmatrix}^\top, \text{where}$$
$$D_K = \begin{bmatrix}y_{\chi_1} A_{\phi_1}^K \\ y_{\chi_1} A_{\phi_2}^K \\ \vdots \\ y_{\chi_T} A_{\phi_S}^K\end{bmatrix} \;\;;\;\; D_B = \begin{bmatrix}y_{\chi_1} A_{\phi_1}^B \\ y_{\chi_1} A_{\phi_2}^B \\ \vdots \\ y_{\chi_T} A_{\phi_S}^B\end{bmatrix}.$$

The product Dx is then bound by vectors $g_{\min}$ and $g_{\max}$, which each contain stiffness and damping constraints for the corresponding points in the gait cycle.

2) Complete Quadratic Program: In summary, the full minimization problem is given by the quadratic program

$$\begin{aligned}\underset{x}{\text{minimize}} \quad & f_1(x) + f_2(x) + f_3(x) + f_4(x) \\ \text{subject to} \quad & g_{\min} \leq Dx \leq g_{\max}\end{aligned} \tag{12}$$

The constants defining the objectives and constraints are provided in Table I. We solve this QP offline using the MOSEK Optimization Toolbox for MATLAB, Version 10.0 [21]. The solution is then saved and accessed in real time by a computer on the prosthetic leg.

III. Experimental Design

The presented controller was implemented on the powered knee-ankle prosthesis described in [22]. The Hybrid Kinematic-Impedance Controller (HKIC) described in [18] was also tested as a benchmark for comparison with prior works utilizing a separate impedance stance and kinematic swing model. Gait phase was calculated using the algorithm in [18]. Though online task estimation has been shown to be viable [18], each controller in this paper assumed the correct walking task in order to eliminate task estimation as a source of error when comparing the two controllers.

An able-bodied subject (male, 24 years, 75 kg, 188 cm) provided written informed consent in accordance with the Institutional Review Board at the University of Michigan (HUM00166976). The subject wore a bypass adapter on the left side to don the prosthesis and a shoe lift on the right to match lengths of his two legs. He wore a ceiling-mounted safety harness and was provided with handrails on either side of the treadmill. The prosthesis was instrumented to record joint angles, joint torques, and ground reaction forces. The ground reaction forces were used to define stance and swing during post-processing, and the joint angles and torques were compared with able-bodied data to assess biomimicry.

Both controllers were first tested over four inclines ($\pm 10^\circ$ and $\pm 3^\circ$) at a fixed speed (1 m/s). The $\pm 10^\circ$ tests evaluated controller performance on tasks in the training space, while the $\pm 3^\circ$ experiments showed controller performance on tasks outside of the training space. Then, both controllers were tested over five speeds (0.8 m/s to 1.2 m/s in 0.1 m/s increments) at level ground. The 0.8 m/s, 1.0 m/s, and 1.2 m/s conditions served to test algorithm performance on tasks from the training space, while the 0.9 m/s and 1.1 m/s conditions showed performance outside of the training space.

TABLE I

CONSTRAINTS AND OBJECTIVE WEIGHTS FOR THE ANKLE (A) AND KNEE (K)

	λ_1^{ES}	λ_1^{MS}	λ_2^{MS}	$\lambda_2^{\mathrm{HS}^-}$	λ_3	λ_4	λ_5	λ_6	$K_{\mathrm{min}}^{\mathrm{WB}}$	$K_{\mathrm{min}}^{\mathrm{st}}$	$K_{\mathrm{min}}^{\mathrm{sw}}$	$B_{\mathrm{min}}^{\mathrm{st}}$	$B_{\mathrm{min}}^{\mathrm{sw}}$	$K_{\mathrm{max}}^{\mathrm{st}}$	$K_{\mathrm{max}}^{\mathrm{sw}}$	$B_{\mathrm{max}}^{\mathrm{st}}$	$B_{\mathrm{max}}^{\mathrm{sw}}$
A	1.0	1.0	1.0	1.0	0.0	1e-3	4e-3	1e-6	3.0	3.0	1.9	0.01	0.027	∞	∞	∞	0.05
K	0.25	1.0	1.0	10	1e-4	1e-3	0.1	1e-6	2.5	1.7	8e-3	3e-3	8e-3	∞	2.3	∞	∞

Each task was tested twice in succession: once with the FSIC and once with the HKIC. The order of controllers was randomized, and the subject was blinded to which controller was being tested. The subject walked for ninety seconds for each task/controller combination, ensuring at least a minute of steady state walking. To minimize the effect of fatigue, we enforced a mandatory one-minute rest period between tasks, with more rest allowed if desired. Footage of the experiments is available in the supplemental video.

IV. RESULTS AND DISCUSSION

Fig. 1 shows the results of the experiments. We used linear interpolation to generate able-bodied reference torques and angles for tasks that are not in the dataset. Tables II and III show normalized root mean square error (NRMSE) values relative to able-bodied kinetics/kinematics. The RMSEs were normalized by the range of the corresponding able-bodied data. Note that the plots and NRMSEs for the joint moments are only provided for stance, as swing period torques should not be judged by their biomimicry (as mentioned when describing the swing objectives of the control method).

Although qualitative comparisons between the FSIC and able-bodied trajectories in Fig. 1 show many parallels, they also indicate differences that should be analyzed. Some of these discrepancies can be attributed to the subject's deviation from the dataset average and the use of a bypass in these experiments, but others may be caused by the control strategy. In particular, we noticed that the knee moment trajectories were farther from able-bodied data than the other three recorded values. This is partially due to the swing objective, the periodicity of the parameters, and the swing-stance transition (Section II-B.7). During swing, the equilibrium angle was driven to able-bodied kinematics. The periodicity of both θ_{eq} and able-bodied kinematics resulted in the two values closely matching during early stance as well. Since stiffness stayed low during swing, it was also low at heel strike. These two circumstances drove the $K(\theta_{\mathrm{eq}} - \theta)$ term in the impedance model close to zero, resulting in smaller overall torques. The reduction in the knee's torque objective weight during early stance meant that this behavior was not punished. The effect is visible in the knee moment plots, as the FSIC's knee moments are generally lower than able-bodied knee moments at heel strike. These conditions were understood when designing the controller and were chosen over the alternative of high stiffnesses and/or non-biomimetic joint angles in late swing. Furthermore, the experiments showed no practical effect of this circumstance, as the subject did not feel any discomfort at heel strike. Note that this problem is not as prevalent in the ankle, as ankle moments are naturally close to zero at heel strike.

Comparing the two controllers shows the viability of the FSIC. When comparing NRMSEs across all tasks, ankle angle NRMSEs are, on average, smaller by 0.1%, ankle stance torque NRMSEs for the FSIC are 1% larger, knee angle NRMSEs are 3% larger, and knee stance torque NRMSEs are 8% larger. All numeric comparisons presented in this section are given as percentage points (i.e., the HKIC had an average ankle angle NRMSE of 15.5% and the FSIC had one of 15.4%, resulting in the 0.1% decrease reported above). These values indicate comparable biomimetic performance for all the data but the knee stance torques (which are still within 10%), showing that the unified model performs with similar efficacy as the benchmark HKIC.

Interestingly, there is a noticeable difference in performance between the incline and speed tasks. When comparing NRMSE averages across the five incline tasks (Table II), the ankle angle NRMSEs for the FSIC are 2% smaller, the ankle stance torque NRMSEs are 0.3% larger, the knee angle NRMSEs are 0.4% larger, and the knee stance torque NRMSEs are 3% larger. The negligible magnitude of these differences indicate equivalency in biomimicry between the two control methods across the incline tasks. However, this is contrasted by the results in the speed tasks, particularly at the knee. For these tasks, the ankle angle NRMSEs had an average increase of 2% for the FSIC, ankle stance torque NRMSEs increased 3%, the knee angle NRMSEs increased 6%, and the knee moment NRMSEs increased 14%.

These experiments showed us various limitations we would like to address in future work. First, we aim to close the final gap between the FSIC and the HKIC, with the goal of ultimately surpassing the HKIC in biomimicry. Given that the only joint/task combination showing a nontrivial decrease in performance is the knee during the speed tasks, this will be our primary area of focus. After this, we will run tests with amputee participants in order to get a sense of the clinical viability of this control method.

V. CONCLUSIONS

The presented control method unified the entire stride of a powered knee-ankle prosthesis under a single continuous model, distinguishing it from previous efforts that utilized separate models and transition criteria to describe stance and swing. The Full Stride Impedance Controller was validated with bypass walking experiments and showed promising levels of biomimicry across a continuum of speed and incline walking conditions. When tested against a state-of-the-art hybrid impedance-kinematic control method, the proposed control method generated joint kinematics and kinetics that displayed a comparable similarity to able-bodied data while having a simpler model architecture.

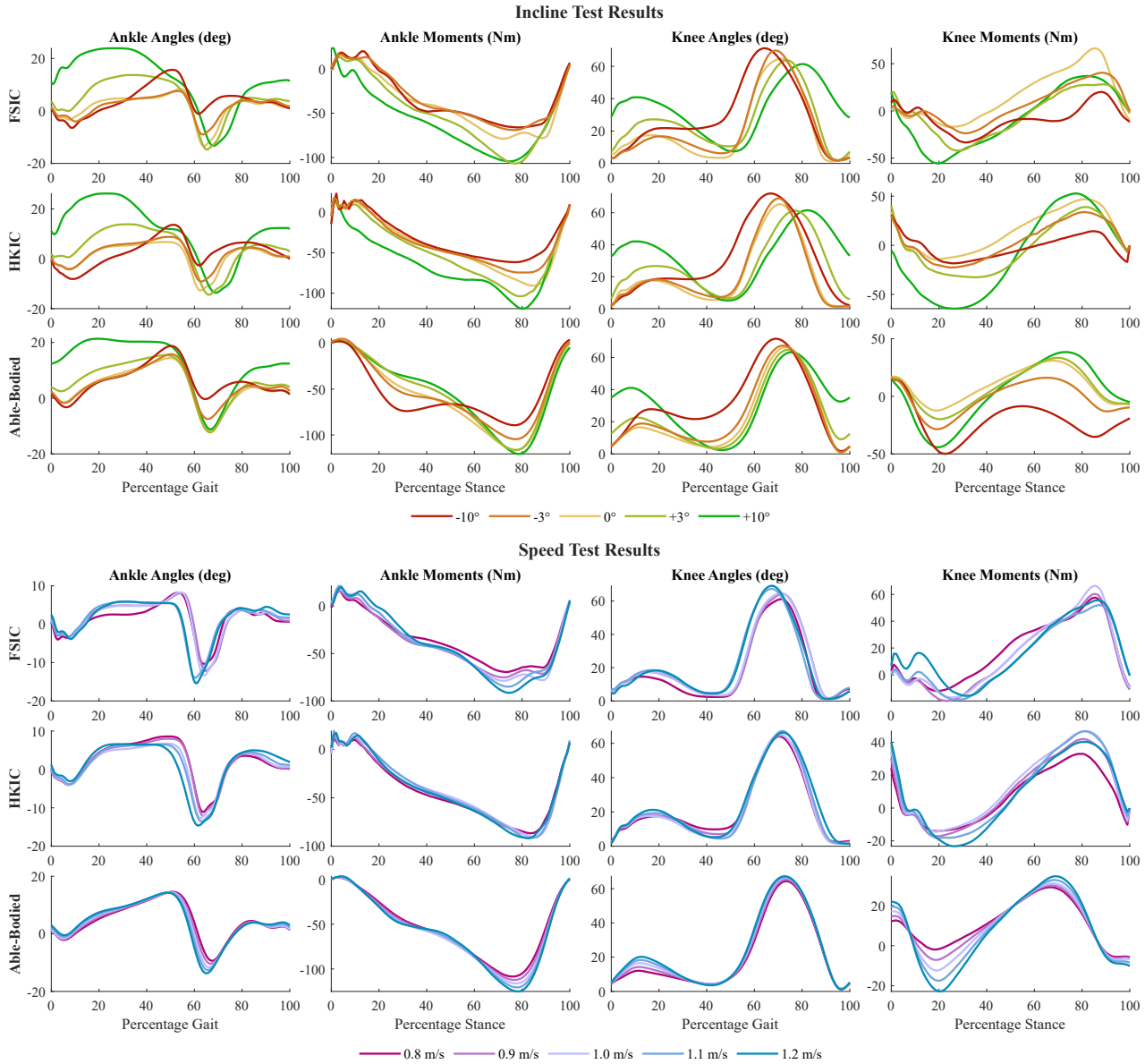

Fig. 1. Plots of inter-stride averages from the experiments for each controller. Inter-subject averages from [2] are shown for the able-bodied trajectories. Note that joint angles are plotted over the entire gait cycle, whereas joint moments are plotted over the stance period.

TABLE II

NORMALIZED ROOT MEAN SQUARE ERROR VALUES ACROSS INCLINE TASKS

	1.0 m/s, −10°		1.0 m/s, −3°		1.0 m/s, 0°		1.0 m/s, 3°		1.0 m/s, 10°	
	FSIC	HKIC	FSIC	HKIC	FSIC	HKIC	FSIC	HKIC	FSIC	HKIC
Ankle Angles (%)	14.37	21.99	18.67	15.79	15.26	16.80	7.55	8.85	9.05	13.47
Ankle Stance Torques (%)	29.65	30.44	22.85	18.53	19.58	18.55	6.52	7.56	10.83	12.87
Knee Angles (%)	10.26	7.68	8.71	10.61	11.74	10.62	12.31	10.88	11.49	12.72
Knee Stance Torques (%)	35.18	38.06	50.16	38.71	52.87	36.99	40.76	40.27	22.11	31.35

TABLE III

NORMALIZED ROOT MEAN SQUARE ERROR VALUES ACROSS SPEED TASKS

	0.8 m/s, 0°		0.9 m/s, 0°		1.0 m/s, 0°		1.1 m/s, 0°		1.2 m/s, 0°	
	FSIC	HKIC	FSIC	HKIC	FSIC	HKIC	FSIC	HKIC	FSIC	HKIC
Ankle Angles (%)	19.75	14.41	15.23	13.94	15.26	16.80	20.06	16.09	18.54	17.75
Ankle Stance Torques (%)	20.91	14.21	18.42	16.03	19.58	18.55	18.07	17.69	17.94	15.74
Knee Angles (%)	15.17	12.18	11.22	9.58	11.74	10.62	19.91	8.39	17.13	5.71
Knee Stance Torques (%)	57.91	37.34	57.22	41.79	52.87	36.99	41.96	34.22	40.71	28.08

REFERENCES

[1] J. Camargo, A. Ramanathan, W. Flanagan, and A. Young, "A comprehensive, open-source dataset of lower limb biomechanics in multiple conditions of stairs, ramps, and level-ground ambulation and transitions," *J. Biomechanics*, vol. 119, p. 110320, 2021.

[2] E. Reznick, K. R. Embry, R. Neuman, E. Bolívar-Nieto, N. P. Fey, and R. D. Gregg, "Lower-limb kinematics and kinetics during continuously varying human locomotion," *Scientific Data*, vol. 8, no. 1, p. 282, Oct 2021.

[3] R. L. Waters, J. Perry, D. Antonelli, and H. Hislop, "Energy cost of walking of amputees: the influence of level of amputation," *JBJS*, vol. 58, no. 1, 1976.

[4] S. M. Jaegers, J. H. Arendzen, and H. J. de Jongh, "Prosthetic gait of unilateral transfemoral amputees: A kinematic study," *Archives of Physical Medicine and Rehabilitation*, vol. 76, no. 8, pp. 736–743, 1995.

[5] D. Quintero, D. J. Villarreal, D. J. Lambert, S. Kapp, and R. D. Gregg, "Continuous-phase control of a powered knee–ankle prosthesis: Amputee experiments across speeds and inclines," *IEEE Trans. Robotics*, vol. 34, no. 3, pp. 686–701, 2018.

[6] K. Embry, D. Villarreal, R. Macaluso, and R. Gregg, "Modeling the kinematics of human locomotion over continuously varying speeds and inclines," *IEEE Trans. Neural Systems and Rehabilitation Engineering*, vol. PP, pp. 1–1, 11 2018.

[7] T. K. Best, K. R. Embry, E. J. Rouse, and R. D. Gregg, "Phase-variable control of a powered knee-ankle prosthesis over continuously varying speeds and inclines," in *2021 IEEE/RSJ Int. Conf. Intelligent Robots and Systems (IROS)*, 2021, pp. 6182–6189.

[8] N. Hogan, "Impedance Control: An Approach to Manipulation: Part I—Theory," *J. Dynamic Systems, Measurement, and Control*, vol. 107, no. 1, pp. 1–7, 03 1985.

[9] H. Lee, E. J. Rouse, and H. I. Krebs, "Summary of human ankle mechanical impedance during walking," *IEEE J. Translational Engineering in Health and Medicine*, vol. 4, pp. 1–7, 2016.

[10] J. Won and N. Hogan, "Stability properties of human reaching movements," *Experimental Brain Research*, vol. 107, no. 1, pp. 125–136, Nov 1995.

[11] E. Burdet, R. Osu, D. W. Franklin, T. E. Milner, and M. Kawato, "The central nervous system stabilizes unstable dynamics by learning optimal impedance," *Nature*, vol. 414, no. 6862, pp. 446–449, Nov 2001.

[12] A. H. Shultz, B. E. Lawson, and M. Goldfarb, "Variable cadence walking and ground adaptive standing with a powered ankle prosthesis," *IEEE Trans. Neural Systems and Rehabilitation Engineering*, vol. 24, no. 4, pp. 495–505, 2016.

[13] K. Bhakta, J. Camargo, P. Kunapuli, L. Childers, and A. Young, "Impedance Control Strategies for Enhancing Sloped and Level Walking Capabilities for Individuals with Transfemoral Amputation Using a Powered Multi-Joint Prosthesis," *Military Medicine*, vol. 185, no. Supplement_1, pp. 490–499, 12 2019.

[14] B. E. Lawson, J. Mitchell, D. Truex, A. Shultz, E. Ledoux, and M. Goldfarb, "A robotic leg prosthesis: Design, control, and implementation," *IEEE Robotics Automation Magazine*, vol. 21, no. 4, pp. 70–81, 2014.

[15] W. Hong, V. Paredes, K. Chao, S. Patrick, and P. Hur, "Consolidated control framework to control a powered transfemoral prosthesis over inclined terrain conditions," in *2019 Int. Conf. Robotics and Automation (ICRA)*, 2019, pp. 2838–2844.

[16] N. A. Kumar, W. Hong, and P. Hur, "Impedance control of a transfemoral prosthesis using continuously varying ankle impedances and multiple equilibria," in *2020 IEEE Int. Conf. Robotics and Automation (ICRA)*, 2020, pp. 1755–1761.

[17] N. Anil Kumar, S. Patrick, W. Hong, and P. Hur, "Control framework for sloped walking with a powered transfemoral prosthesis," *Frontiers in Neurorobotics*, vol. 15, p. 790060, 2022.

[18] T. K. Best, C. G. Welker, E. J. Rouse, and R. D. Gregg, "Data-driven variable impedance control of a powered knee–ankle prosthesis for adaptive speed and incline walking," *IEEE Trans. Robotics*, vol. 39, no. 3, pp. 2151–2169, 2023.

[19] R. J. Cortino, T. K. Best, and R. D. Gregg, "Data-Driven Phase-Based Control of a Powered Knee-Ankle Prosthesis for Variable-Incline Stair Ascent and Descent," *IEEE Transactions on Medical Robotics and Bionics*, vol. 6, no. 1, pp. 175 – 188, 2024.

[20] C. G. Welker, T. K. Best, and R. D. Gregg, "Improving sit/stand loading symmetry and timing through unified variable impedance control of a powered knee-ankle prosthesis," in *IEEE Trans. Neural Systems and Rehabilitation Engineering*, 2023.

[21] M. ApS, *MOSEK Optimization Toolbox for MATLAB 10.0.47*, 2023. [Online]. Available: http://docs.mosek.com/10.0/toolbox/index.html

[22] T. Elery, S. Rezazadeh, C. Nesler, and R. D. Gregg, "Design and validation of a powered knee–ankle prosthesis with high-torque, low-impedance actuators," *IEEE Trans. Robotics*, vol. 36, no. 6, pp. 1649–1668, 2020.